

Supporting Information for “Visible Discrimination of Broadband Infrared Light by Dye-Enhanced Upconversion in Lanthanide-Doped Nanocrystals”

*Charles G. Dupuy**, *Thomas L. Allen*, *George M. Williams*, *David M. Schut[†]*

Voxtel Inc., 15985 NW Schendel Ave. Ste. 200, Beaverton OR 97006, USA

(* Address correspondence to: charlesd@voxtel-inc.com

([†]) Current Address: Shoei Electronic Materials Inc., 1110 NE Circle Blvd., Corvallis, OR 97300

TABLE OF CONTENTS:

- A. X-ray Diffraction and HR-TEM Data for Lanthanide-Doped NaYF₄ Nanoparticles
- B. Fourier Transform Infrared (FTIR) Spectroscopy of Nanoparticles
- C. Optical Technique for Assessing Chemical Robustness of Infrared Dyes with Respect to Amine-Containing Siloxane Monomer
- D. Validating the Dye-Attach Procedure and Measuring Förster Resonance Energy Transfer (FRET)

E. Efficiency of Dye-Attach and Calculations of the Number of Dye Molecules per Nanoparticle Monomer

F. Larger Renderings of TEM Images

A. X-RAY DIFFRACTION AND HR-TEM DATA FOR LANTHANIDE-DOPED NaYF₄ NANOPARTICLES

Figure S1 shows the x-ray diffraction pattern of NaYF₄:Yb³⁺,Tm³⁺ nanoparticles synthesized at 315 °C. The angular positions of the diffraction peaks match the Joint Committee on Powder Diffraction Standard (JCPDS) 28-1192 for hexagonal NaYF₄, but the relative amplitudes are different, which we attribute to self-assembly (preferential alignment) of the hexagonal rods in the measured sample. The high-resolution transmission electron microscope (HR-TEM) images in Figure S2 and Figure S3 show highly-uniform hexagonal rods, which have grown to a 75 nm short-axis dimension during the growth time of 80 minutes. The image in Figure S2, left, is the fast Fourier transform of the diffraction pattern from a single nanocrystal, which confirms the well-defined hexagonal crystalline structure. Higher resolution renderings of the TEM images can be found in Section F.

The HR-TEM image in Figure S3 shows an approximately 12 nm thick silica shell comprised of a thin inner, amine-functionalized silica shell with attached infrared dye, which is further encapsulated with a thick, nonfunctionalized silica shell. The majority of results in this report are taken with smaller nanoparticles having only the inner shell. A TEM image comparing thin and thick silica shells can be found in the paper “Visible Discrimination of Broadband Infrared Light by Dye-Enhanced Upconversion in Lanthanide-Doped Nanocrystals,” Figure 5.

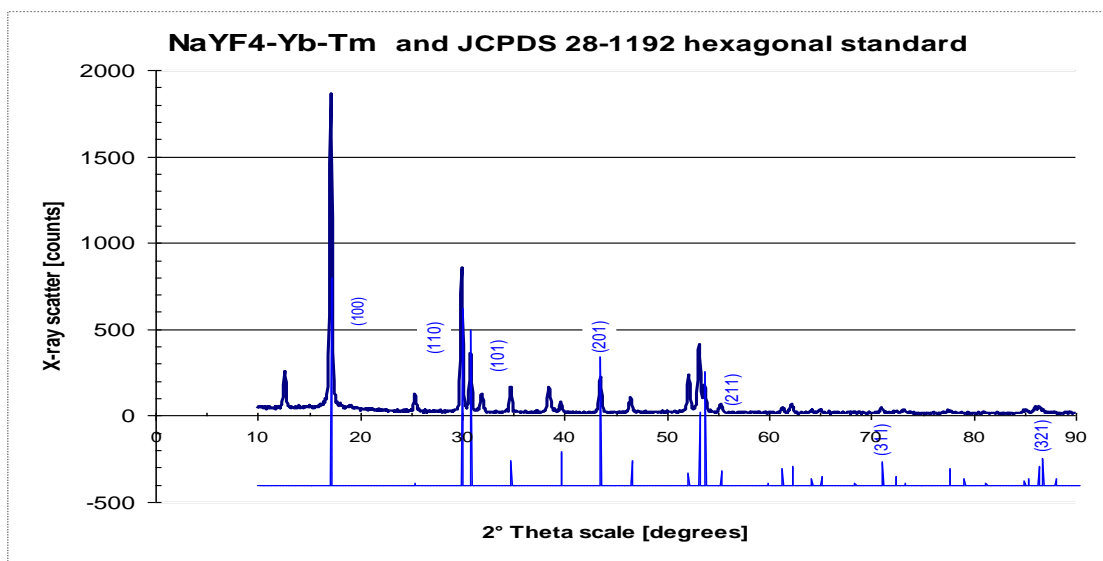


Figure S1. X-ray scattering data from $\text{NaYF}_4:\text{Yb}^{3+}, \text{Tm}^{3+}$ (black curve). In blue is the reference data for hexagonal NaYF_4 . The mismatch in relative peak heights between the sample under test and the reference file is consistent with an ordered stacking of crystallites in the sample under test, as is seen in the TEM images of Figure S2.

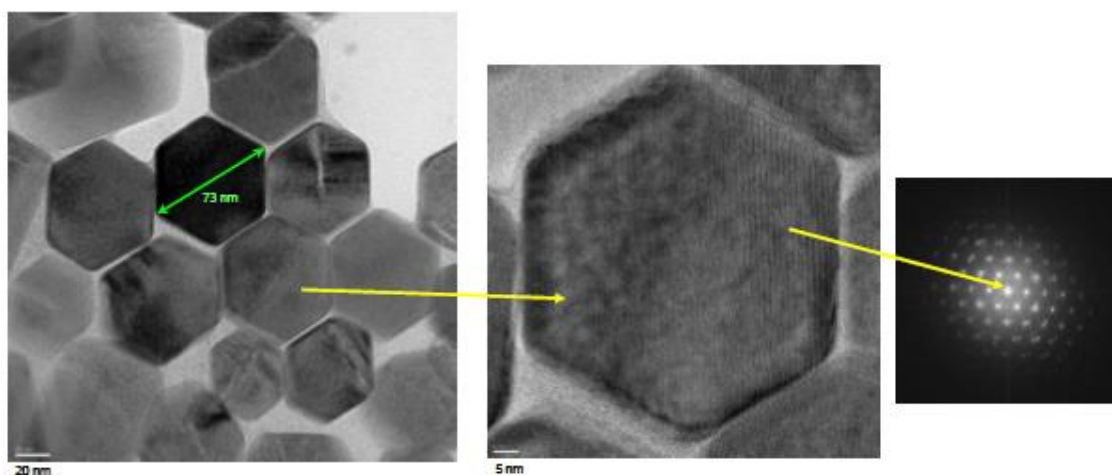


Figure S2. HR-TEM images of $\text{NaYF}_4:\text{Yb}^{3+}, \text{Tm}^{3+}$ nanoparticles synthesized at 315 °C, showing hexagonal crystals with ~75 nm short-axis dimension. The left image is the fast Fourier transform of the diffraction pattern from a single nanocrystal.

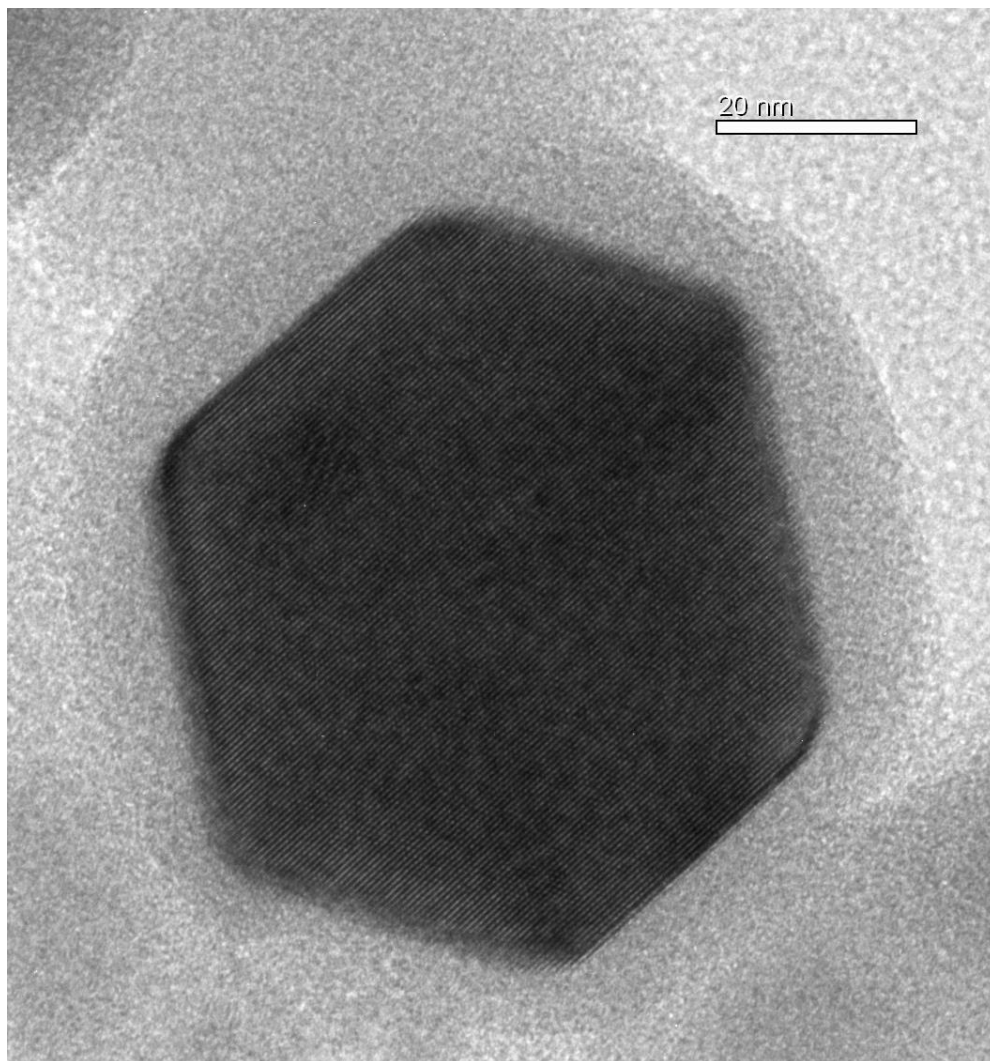


Figure S3. HR-TEM image of a 12 nm silica shell encapsulating a single ~75 nm $\text{NaY}_{0.747}\text{Yb}_{0.25}\text{Tm}_{0.003}\text{F}_4$ nanocrystal. The silica shell includes the DY-831 infrared dye, which is not discernible in the image.

B. FOURIER TRANSFORM INFRARED (FTIR) SPECTROSCOPY OF NANOPARTICLES

The FTIR spectra of Figure S4 show the changes in the organic groups on NaYF_4 nanoparticles as the process flows from the as-synthesized particles with oleic acid ligands to the nanoparticles functionalized with amine groups for subsequent reaction with the functionalized dye to form an amide bond linking the nanoparticle to the dye molecule. The results are for Tm doped NaYF_4

nanoparticles, but are expected to be the same for all of the lanthanide-doped NaYF₄ nanoparticles used in this report. The FTIR data was recorded using dry nanoparticles pressed in KBr pellets.

Drawing heavily on the analysis of Hu *et al.* [1], we assign the bands at 2924 and 2853 cm⁻¹ in the top curve to the asymmetric and symmetric stretching vibrations of methylene groups (CH₂) in the long alkyl chain of oleic acid, while the bands at 1558 cm⁻¹ is assigned to the asymmetric COO-Na stretching modes [2]. As shown in the middle and lower curves, the bands associated with oleic acid disappear when the nanoparticles are reacted with either TEOS (middle curve) or a combination of TEOS and APS (bottom curve). The middle and lower curves show a strong band around 1075 cm⁻¹ corresponding to the Si-O-Si asymmetric stretching vibration and a band at 460 cm⁻¹ corresponding to the Si-O deformation vibration. The N-H stretching band for amines is expected in the range of 3000-3500 cm⁻¹, while the N-H bend is expected around 1600 cm⁻¹, but neither was clearly discernible in the lower spectrum. The broad band around 3500 cm⁻¹ in the middle spectrum is attributed to water.

As was the case in the report by Hu *et. al* [1], the FTIR data confirms the displacement of the synthesis ligand and the formation of a silane shell, but does not identify the presence of the expected amine functional group. Under the assumption that the FTIR signal from the amine groups was lost in the background, an experiment for future consideration would be to make KBr pellets with higher concentrations of nanoparticles, and to make three different silica shells with slightly different signatures using the primary, secondary, and tertiary forms of APS. One would then look for small shifts in FTIR peak positions in the range of 3000–3500 cm⁻¹ corresponding to the three forms of APS.

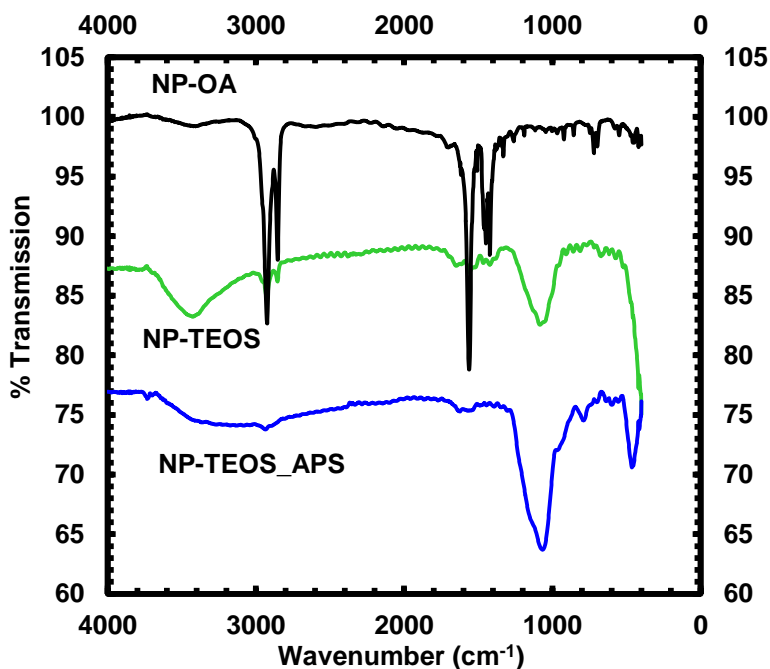


Figure S4. FTIR spectra of: (top) as-synthesized nanoparticles with oleic acid ligands; (middle) after reaction with TEOS to form a silane shell; (bottom) after reaction with a combination of TEOS and APS to functionalize with amine groups. The middle and bottom curves were offset vertically for better viewing.

C. OPTICAL TECHNIQUE FOR ASSESSING CHEMICAL ROBUSTNESS OF INFRARED DYES WITH RESPECT TO AMINE-CONTAINING SILOXANE MONOMER

Some of the infrared dyes are susceptible to attack by the primary amine group of the functionalized siloxane (3-aminopropyl) trimethoxysilane (APS), but are found to be sufficiently robust to the related, but less reactive, secondary and tertiary amines, [3-(methylamino)propyl] trimethoxysilane and (3,3-dimethylaminopropyl) trimethoxysilane, respectively. The chemical stability of the infrared dye in the presence of the linker molecules is tracked by measuring the

ultraviolet-visible-near infrared (UV-VIS-NIR) absorption as a function of time following injection of the amine. A drop in the absorption of the dye after adding the linker indicated a degradation of the dye; the rate at which the absorption dropped was a relative measurement of chemical robustness. Figure S4 shows the time evolution of the UV-VIS-NIR absorption of the DY-831 infrared dye following addition of various amine-functionalized linker molecules. The DY-831 infrared dye degrades immediately in the presence of the APS primary amine and the secondary amine, but is moderately stable (50% degradation over two days) in the presence of the tertiary amine. Tight bonding of the dye to the nanoparticle is confirmed by repeated washes of the dye-nanoparticle composite until the elute is clear and colored nanoparticles remain.

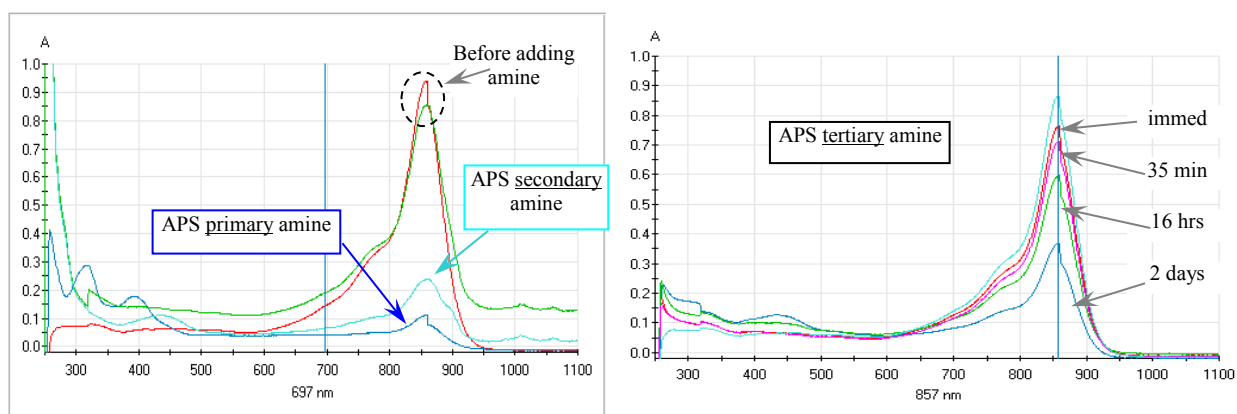


Figure S5. Chemical stability of NHS-functionalized form of DY-831 dye in presence of amine-bearing linker molecules, as measured by the time evolution of visible-infrared absorption spectrum: Absorption spectrum before and immediately after addition of the primary or secondary amines (left) with degradation occurring in the ~3 minutes it takes to make the measurements; and much improved stability in the presence of the tertiary amine linker (right).

The optical stability technique is used for screening infrared dyes with 801 nm emission. Several dyes show less than 5% degradation after a week in tertiary amine. The most robust infrared dye, DLS-776A, is stable in presence of the primary amine linker, but still requires the

modified silica functionalization procedure to avoid exposure to the base-catalyzed condensation reaction. Figure S6 shows the photophysical properties of the DLS-776A dye.

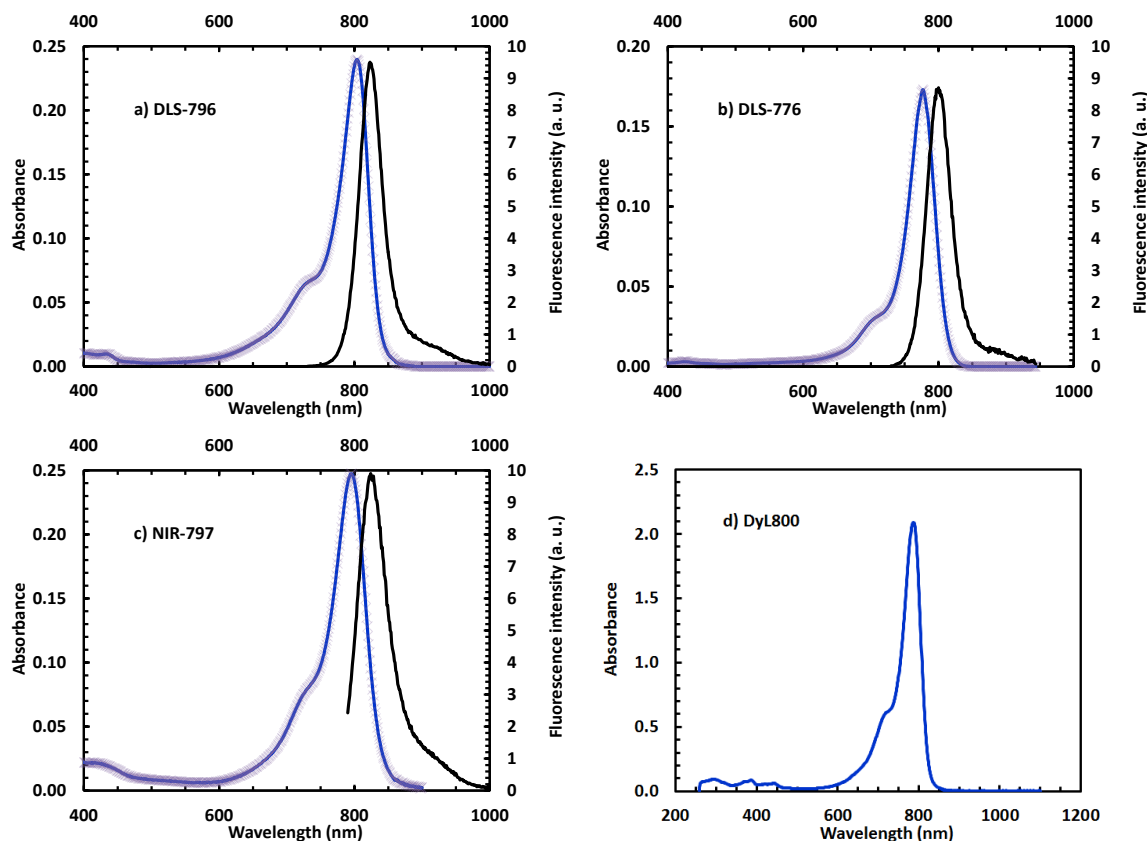


Figure S6. The absorbance spectrum and fluorescence emission spectrum for alternate dyes: a) DLS-796 in ethanol with an absorptivity of $303 \text{ L g}^{-1} \text{ cm}^{-1}$ at 796 nm and a fluorescence peak at 804 nm; b) DLS-776 in ethanol with an absorptivity of $350 \text{ L g}^{-1} \text{ cm}^{-1}$ at 776 nm and a fluorescence peak at 800 nm ; c) NIR-797 in methanol with an absorptivity of $290 \text{ L g}^{-1} \text{ cm}^{-1}$ at 797 nm and a fluorescence peak at 825 nm; d) absorption spectrum of DyL800 in DMSO using the concentrated solution labeled 10x in the picture inset of Figure 4 of the primary document The measurements of d) DYL800 were made in a 1 mm sample cell. The other data measured in 1 cm sample cells.

D. VALIDATING THE DYE-ATTACH PROCEDURE AND MEASURING FÖRSTER RESONANCE ENERGY TRANSFER (FRET)

Optical tests are performed to validate the success of the multistep procedure of functionalizing the nanoparticles and reacting with the dye, as well as efficient energy transfer between nanoparticle and dye. In the early stages of this investigation, we planned to use the dye-attach and encapsulation procedures described by Van Blaaderen and Vrij,^{Error! Bookmark not defined.} which consisted of reacting the amine-containing siloxane monomer with the dye *before* the condensation step, followed by a further encapsulation of the thin dye-functionalized silica shell by a nonfunctionalized silica shell made from tetraethylorthosilicate (TEOS). This procedure has the dual advantage of placing the dye closer to the nanoparticle surface and creating an external shell that can be subsequently functionalized for compatibility with the future host matrix for the nanocomposite. This process flow works well for the robust fluorescein-free acid (FIFA) dye, but was found to degrade certain less-robust infrared dyes.

The optical testing configuration was the more traditional FRET from the nanoparticle to the dye. The optical signature of success is a decrease in the upconverted visible light of the nanoparticle due to absorption by the attached dye, followed by fluorescence emission from the dye. The upconverting nanoparticle is NaYF₄ doped with Yb³⁺ activator and a mixture of Tm³⁺ and Er³⁺ emitters. Excitation at 975 nm produces a series of upconversion lines in the blue and green, which are well matched to the visible FIFA dye. In this test configuration, the attached FIFA dye absorbs the 474 nm light (and to a lesser degree the 520 – 530 nm light) from the upconverting nanoparticle, then produces the characteristic emission of FIFA dye, 500 – 650 nm, which overlays and partly masks the upconverted emission lines at 540 – 560 nm. Figure S7 is a composite plot showing the upconversion spectrum for NaYF₄:Yb³⁺,Tm³⁺,Er³⁺ with and without

attached FIFA dye, as well as the emission from the $\text{NaYF}_4:\text{Yb}^{3+},\text{Tm}^{3+},\text{Er}^{3+}$ FIFA composite when it is directly excited at the absorption peak of the FIFA dye at 474 nm. Integration of the spectra for nanoparticles with and without attached dye indicate that the upconverted signal at 474 nm is attenuated roughly 65% by energy transfer to the FIFA dye, and up to 35% of that transferred energy is re-emitted as fluorescence from the dye. These results show that highly efficient energy transfer between dye and nanoparticle can be achieved through these process steps. Energy transfer will be less efficient for the process flow, which was modified for the less robust infrared dye, namely attaching the dye to the exterior of the thin silica shell, *i.e.*, at a greater distance from the nanoparticle.

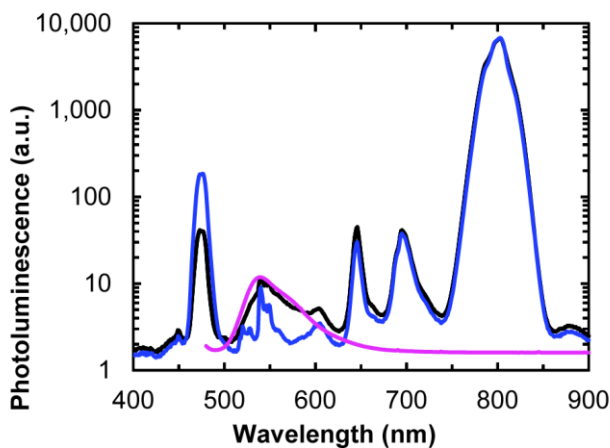


Figure S7. Composite plot, on logarithm scale, showing the upconversion spectra for $\text{NaYF}_4:\text{Yb}^{3+},\text{Tm}^{3+},\text{Er}^{3+}$ with and without attached FIFA dye (black and blue curves respectively), as well as the emission from the $\text{NaYF}_4:\text{Yb}^{3+},\text{Tm}^{3+},\text{Er}^{3+}$ FIFA composite (magenta curve) when it is directly excited at the absorption peak of the FIFA dye at 474 nm.

E. EFFICIENCY OF DYE-ATTACH AND CALCULATIONS OF THE NUMBER OF DYE MOLECULES PER NANOPARTICLE MONOMER

Table S1 shows measurements of the efficiency of dye attachment and calculations of the number of dye molecules per nanoparticle. The nanoparticles were 15 nm ± 4 nm by 25 nm ± 5 nm, (same batch of nanoparticle as shown in the TEM image of Figure 5, right, of the primary article). The nanoparticles were functionalized with the primary amine linker APS. The infrared dye was DLS-796A. The dye manufacturer indicates that the DLS-796A is a cyanine-based dye with a molecular weight of 807, but does not disclose the chemical structure. The photophysical properties of DLS-796A are shown in Figure S5.

The data in Table S1 show that the dye-attach process has an efficiency of up to 10%. Dye attachment starts saturating around 60 dye molecules per nanoparticle. Collectively, these results indicate that the dye-attach process should be carried out with a dye molecules-to-nanoparticle ratio of at least 200:1. The saturation value of 60 dye molecules per 15 nm by 25 nm particle equates to 25 nm² area per molecule, which is 10 times more than one would expect for a molecule with a molecular weight of 807. The saturation may be an indication of steric hindrance of the dye molecules on the amine-functionalized surface of the particle.

Table S1. Ratio of Dye-to-Nanoparticles in Reaction Mix and in Purified Dye-Particle Nanocomposite, and Calculated Attachment Efficiency.

	Solution 1	Solution 2	Solution 3	Solution 4	Solution 5
# of Dye Molecules / Nanocrystal Available During Synthesis	12	18	44	141	461
# of Dye Molecules / Nanocrystal Remaining Attached	0.1	1	5	23	33

% Attachment	1	8	12	16	7
--------------	---	---	----	----	---

The photograph in Figure S8 shows the color change of the dye-attached nanoparticles with increasing dye coverage. The dye-attached particles have been washed 5 – 8 times with ethanol to remove the excess, nonattached dye molecules. Without attached dye, the amine-functionalized nanoparticles appear yellow or light brown. Once the samples have reached about half their maximum dye coverage, they appear green, similar to the dye in solution.

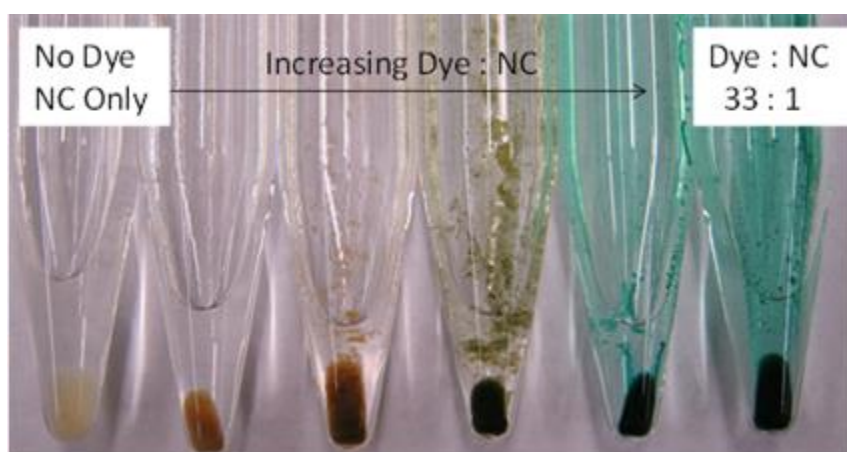


Figure S8. Photograph of dye-particle nanocomposites of Table S1 with increasing loading of the infrared dye DLS-796A. The clear supernate above the nanocomposite shows that the excess, nonattached dye has been removed by the repeated washing with solvent.

The thermogravimetric analysis (TGA) measurements of Figure S9 show that the as-sensitized nanoparticles have ~25% by weight of the synthesis ligand oleic acid, from which one can calculate the weight of bare nanoparticles in a given sample. Figure S10 (as well as “Visible Discrimination of Broadband Infrared Light by Dye-Enhanced Upconversion in Lanthanide-Doped Nanocrystals,” Figure 6) shows the absorption spectra of a calculated weight of 150 mg of bare nanoparticles in 4 mL of hexane.

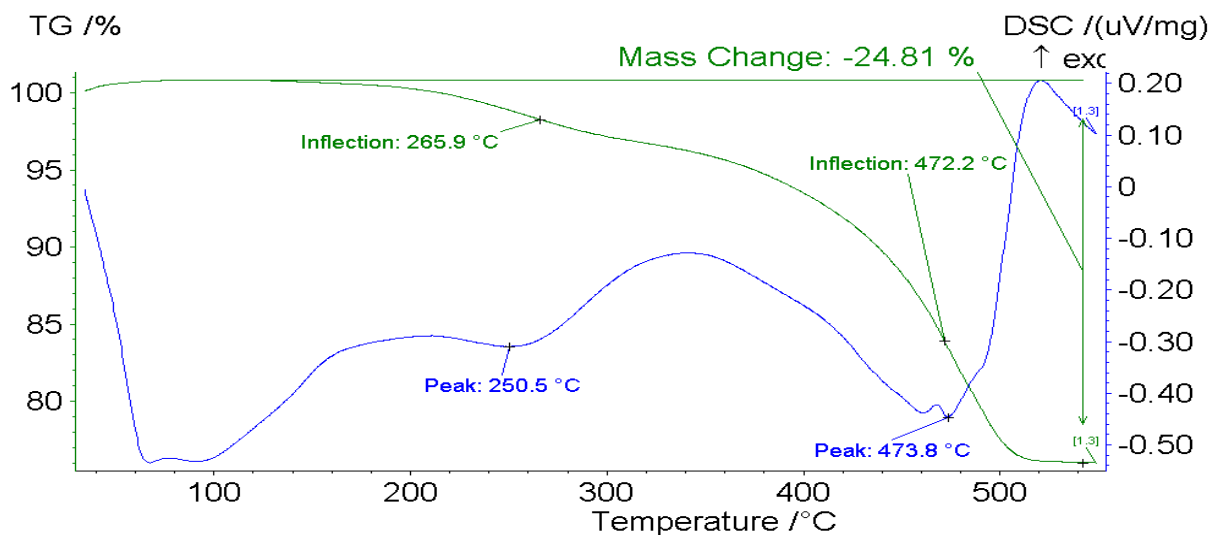


Figure S9. TGA data for oleic-acid-capped NaYF₄ show the weight percent of ligand and bare nanoparticles to be 25% and 75% respectively. The two-component thermal behavior is consistent with loosely and tightly bound oleate ligands, which depart at 270 °C and 470 °C respectively, as described in a recent report by Yang [3].

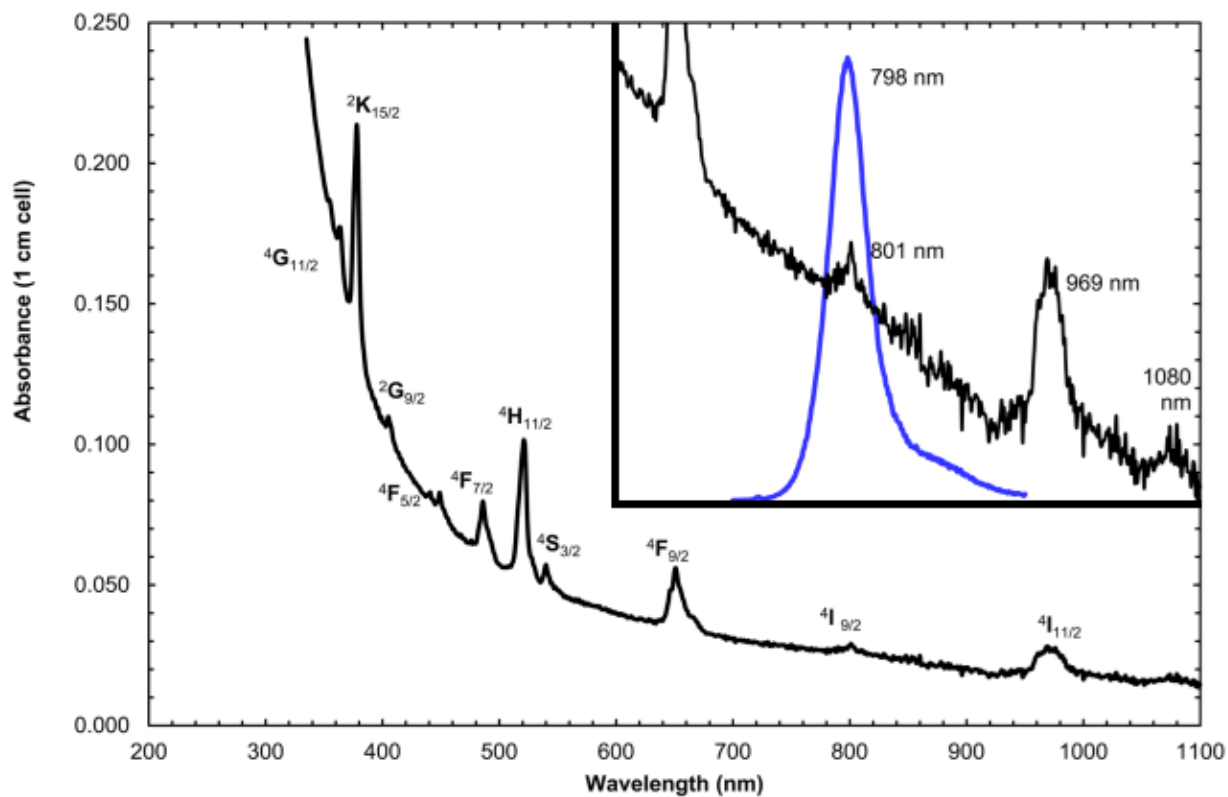


Figure S10. The absorption spectrum in a 1 cm cell of 0.1 M NaYF₄:Er³⁺ in cyclohexane. Transition assignments are derived from Reisfeld and Jørgensen [4]. Inset is a six-fold expansion highlighting the weak absorption at 801 nm, over which is shown the emission spectrum of DyL800 infrared dye.

F. LARGER RENDERINGS OF TEM IMAGES

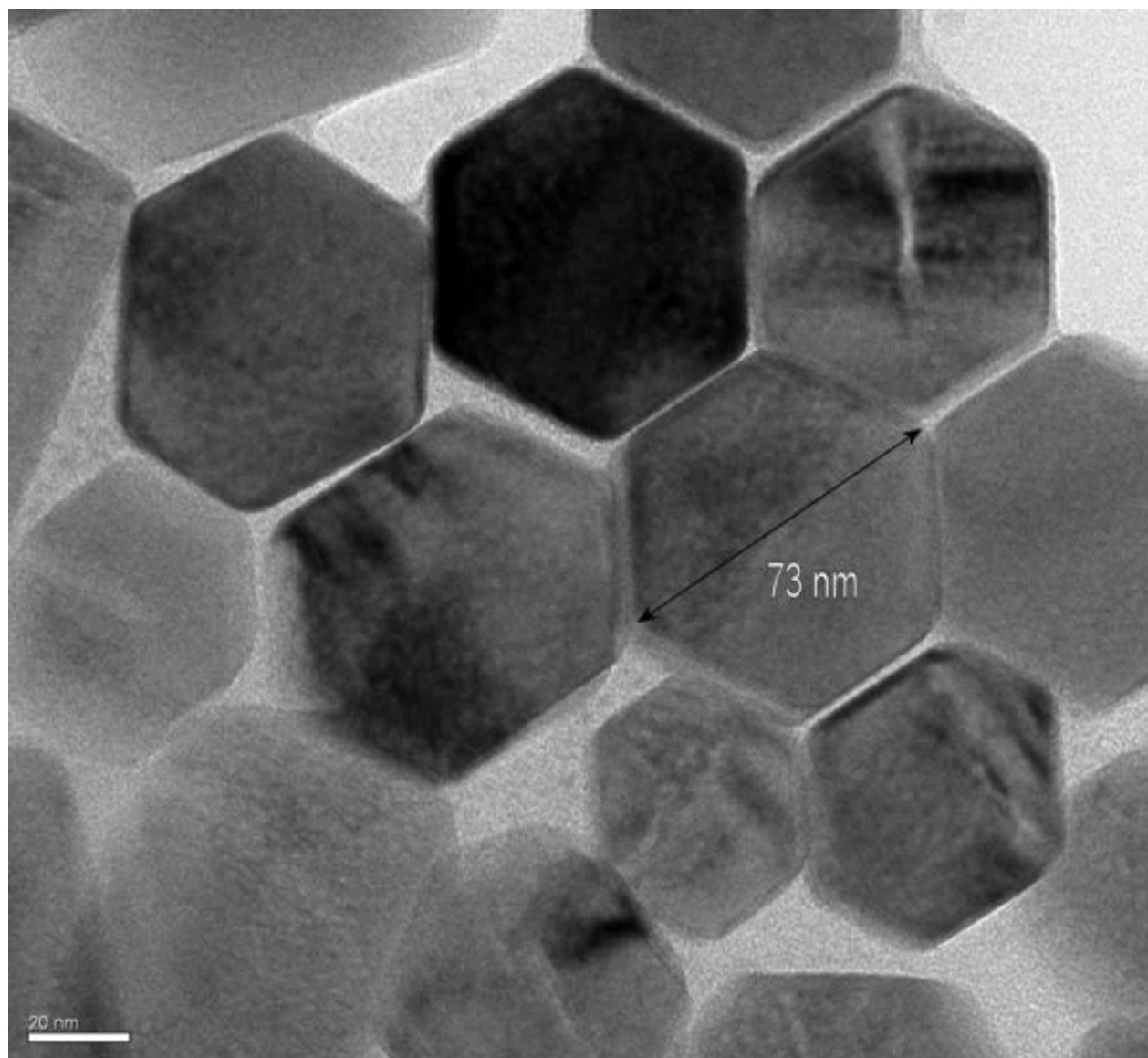


Figure S11. Larger image of Figure 1, right.

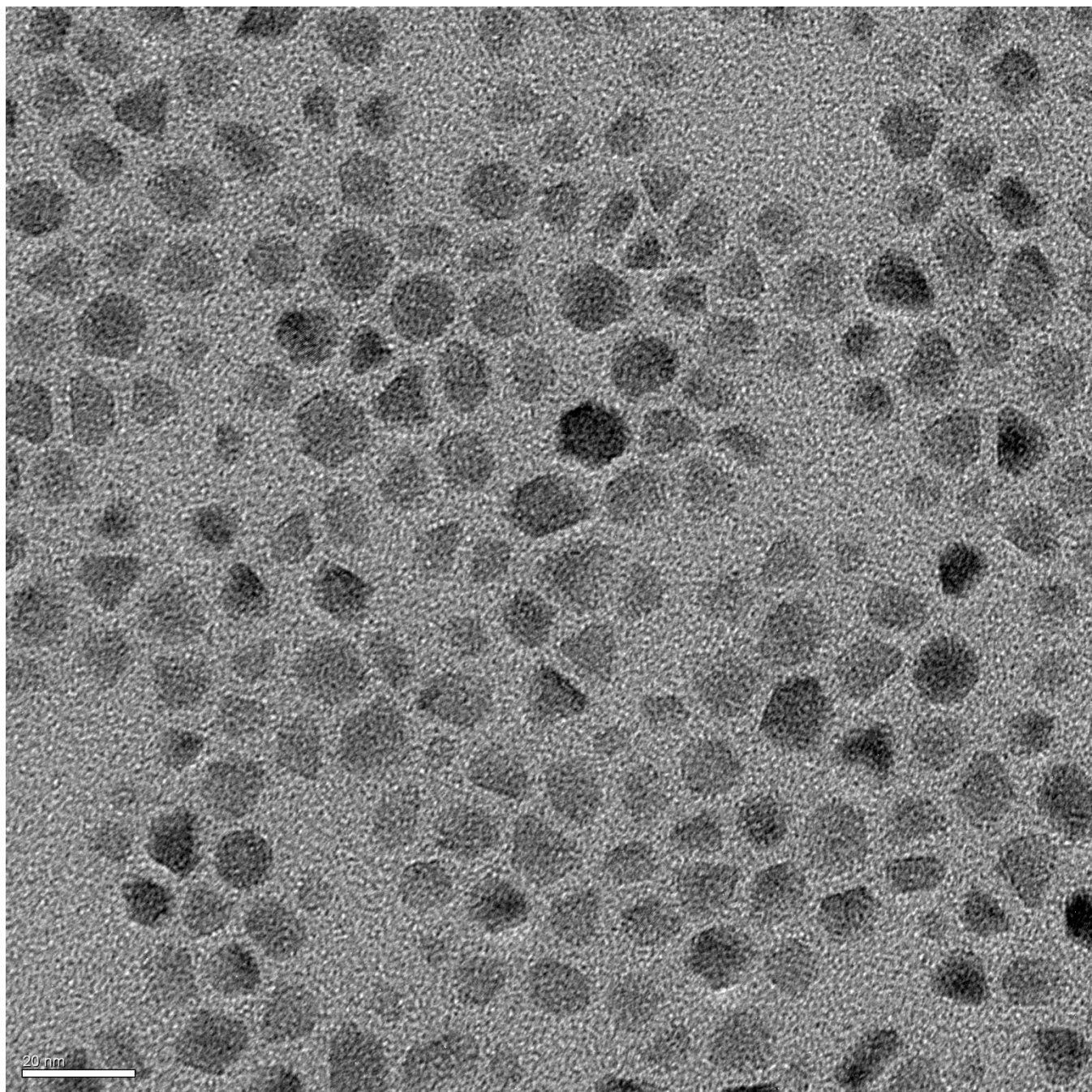


Figure S12. Larger image of Figure 1, left.

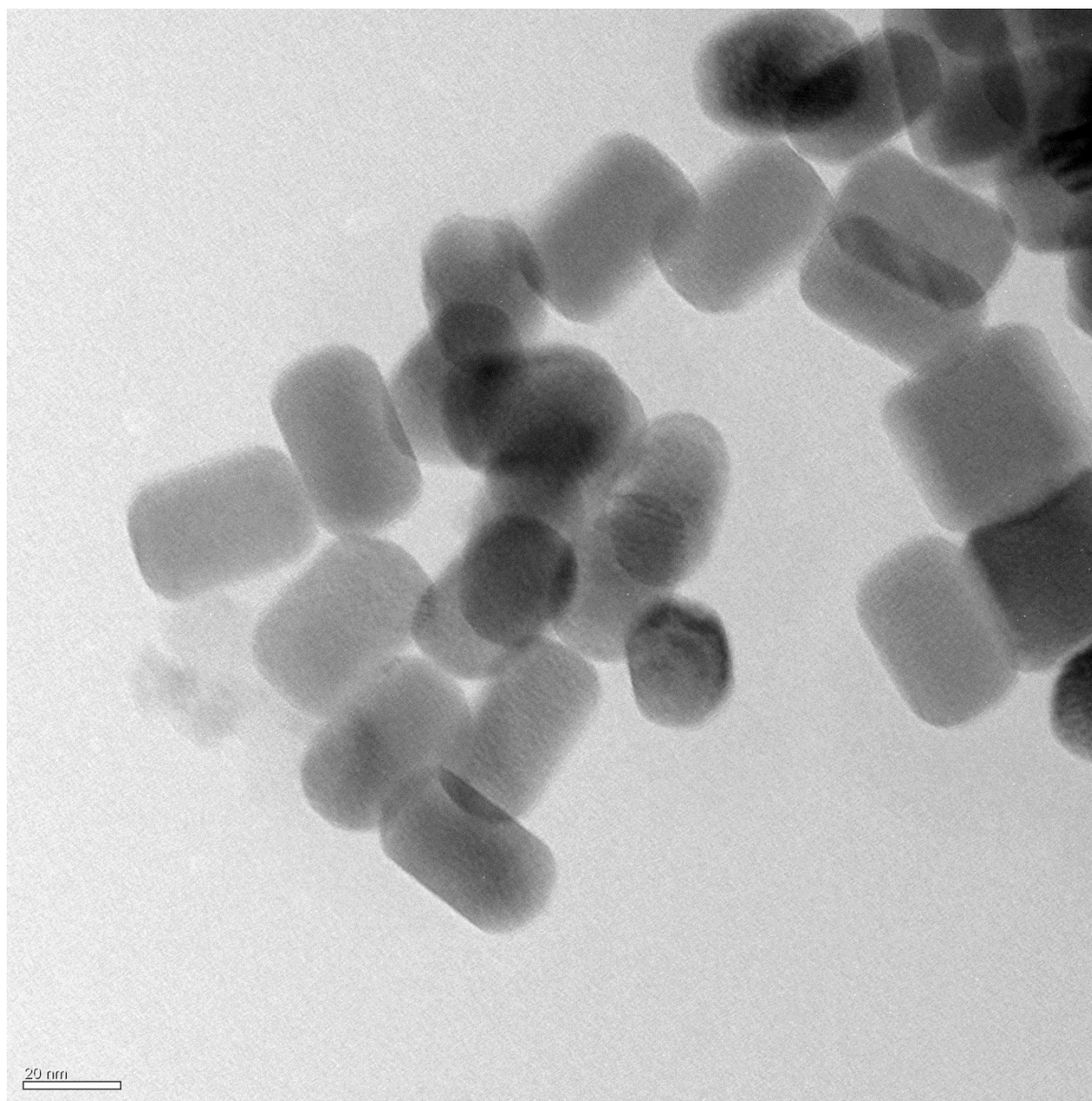


Figure S13. Larger image of Figure 5, right.

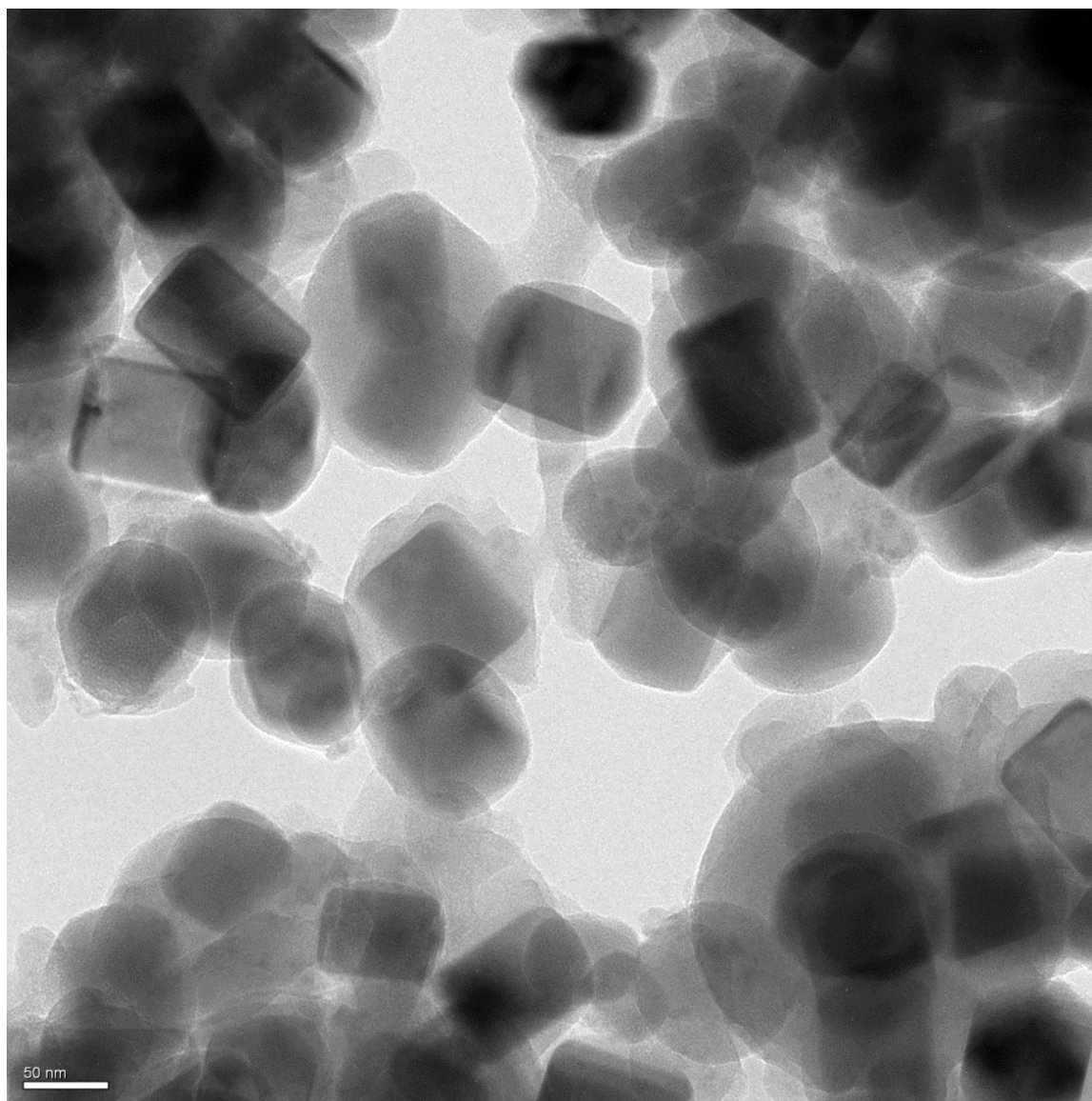


Figure S14. Larger image of Figure 5, left.

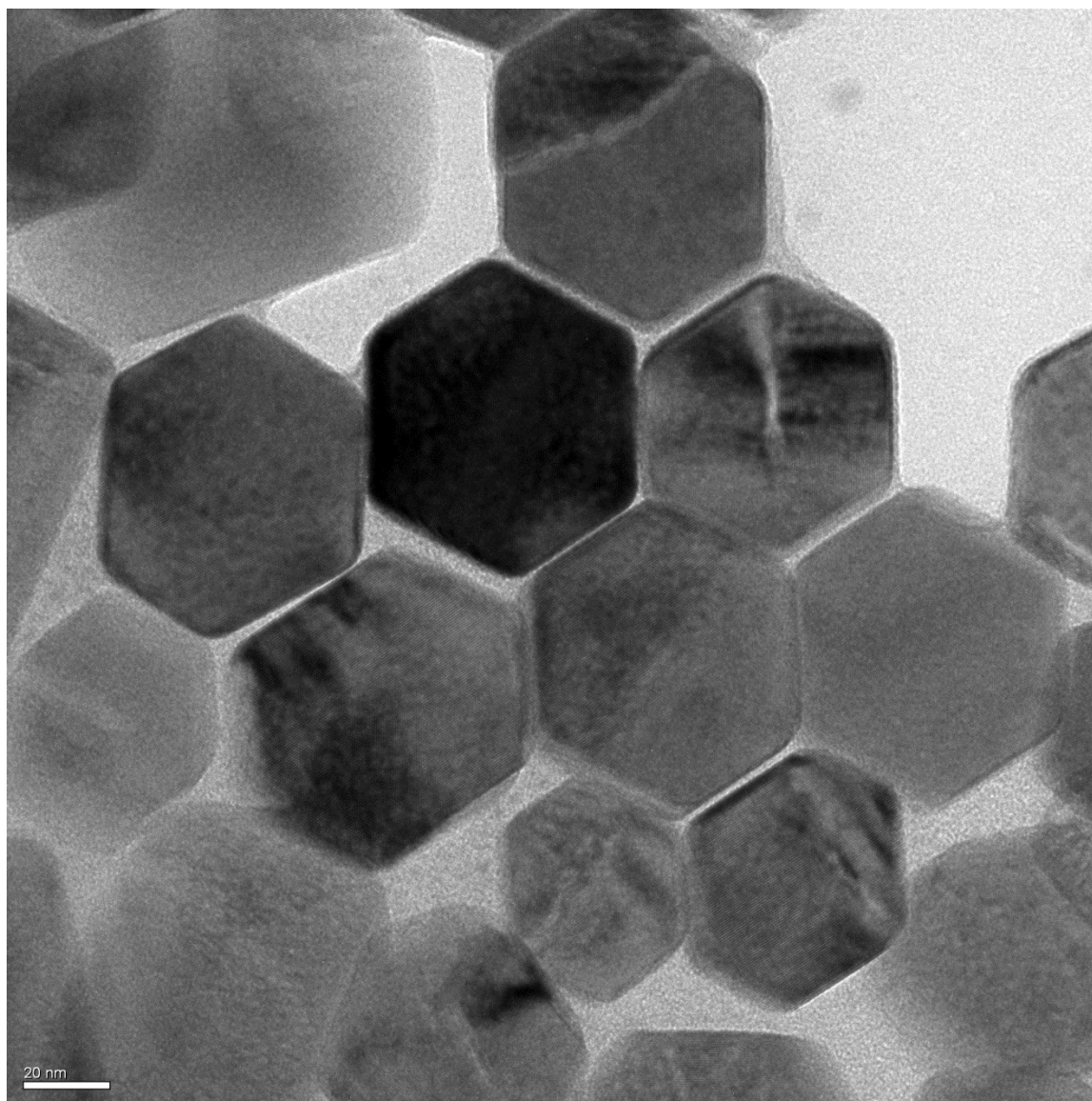


Figure S15. Larger image of Supporting Information Figure S2, left.

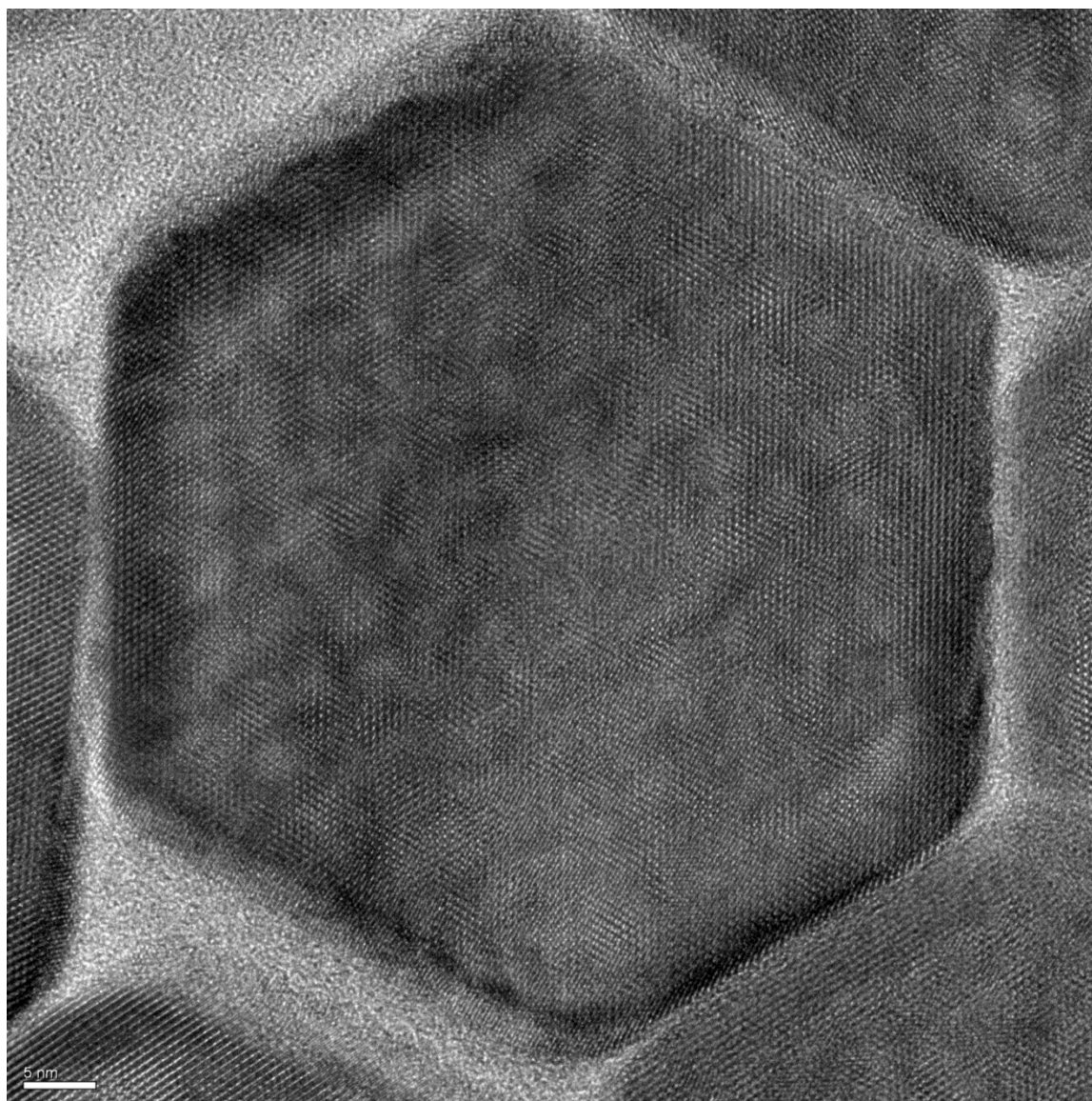


Figure S16. Larger image of Supporting Information Figure S2, middle.

REFERENCES

- [1] Hu, H.; Xiong, L.; Zhou, J.; Li, F.; Cao, T.; Huang, C. Multimodal-Luminescence Core–Shell Nanocomposites for Targeted Imaging of Tumor Cells. *Chem.-A Eur. J.*, **2009** 15(14), 3577-3584.

-
- [2] Lee, D. H.; Condrate Sr, R. A.; Lacourse, W. C. FTIR Spectral Characterization of Thin Film Coatings of Oleic Acid on Glasses, Part II: Coatings on Glass From Different Media Such As Water, Alcohol, Benzene and Air. *J. Mat. Sci.* **2000**, *35*, 4961–4970
- [3] Yang, K.; Peng, H.; Wen, Y.; Li, N. Re-Examination of Characteristic FTIR Spectrum of Secondary Layer in Bilayer Oleic Acid-Coated Fe₃O₄ Nanoparticles. *Appl. Surf. Sci.* **2010**, *256*, 3093–3097.
- [4] Reisfeld, R.; Jørgensen, C. K. Chemical Bonding and Lanthanide Spectra. In *Lasers and Excited States of Rare Earths*. Jørgensen, C. K.; Lappert, M. F.; Lippard, S. J.; Margrave, J. L.; Niedenzu, K.; Nöth, H.; Parry, R. W.; Yamatera, H., Eds.; Springer-Verlag: Berlin, 1977; pp 138–142.